

# Soft Self-labeling and Potts Relaxations for Weakly-Supervised Segmentation

Zhongwen (Rex) Zhang & Yuri Boykov  
University of Waterloo, Canada

z889zhan@uwaterloo.ca, yboykov@uwaterloo.ca

## Abstract

We consider weakly supervised segmentation where only a fraction of pixels have ground truth labels (scribbles) and focus on a self-labeling approach optimizing relaxations of the standard unsupervised CRF/Potts loss on unlabeled pixels. While WSSS methods can directly optimize such losses via gradient descent, prior work suggests that higher-order optimization can improve network training by introducing hidden pseudo-labels and powerful CRF sub-problem solvers, e.g. graph cut. However, previously used hard pseudo-labels can not represent class uncertainty or errors, which motivates soft self-labeling. We derive a principled auxiliary loss and systematically evaluate standard and new CRF relaxations (convex and non-convex), neighborhood systems, and terms connecting network predictions with soft pseudo-labels. We also propose a general continuous sub-problem solver. Using only standard architectures, soft self-labeling consistently improves scribble-based training and outperforms significantly more complex specialized WSSS systems. It can outperform full pixel-precise supervision. Our general ideas apply to other weakly-supervised problems/systems. Code can be found on <https://vision.cs.uwaterloo.ca/code>.

**keywords:** soft pseudo-labels, collision cross-entropy, collision divergence

## 1. Introduction

Full supervision for semantic segmentation requires thousands of training images with complete pixel-accurate ground truth masks. Their high costs explain the interest in weakly-supervised approaches based on image-level class tags [4, 23], pixel-level scribbles [28, 37, 38], or boxes [25]. This paper is focused on weak supervision with scribbles, which we also call *seeds* or *partial masks*. While only slightly more expensive than image-level class tags, scribbles on less than 3% of pixels were previously shown to achieve accuracy approaching full supervision without any modifications of the segmentation models. In contrast, tag supervision typically requires highly specialized systems and complex multi-stage training procedures, which are hard

to reproduce. Our interest in the scribble-based approach is motivated by its practical simplicity and mathematical clarity. The corresponding methodologies are focused on the design of unsupervised or self-supervised loss functions and stronger optimization algorithms. The corresponding solutions are often general and can be used in different weakly-supervised applications.

### 1.1. Scribble-supervised segmentation

Let  $\Omega$  denote a set of image pixels and  $S \subset \Omega$  denote a subset of pixels with ground truth labels, i.e. *seeds* or *scribbles* typically marked by mouse-controlled UI for image annotations. One example of image scribbles is in Fig.4(a). The ground truth label at any given pixel  $i \in S$  is an integer

$$\bar{y}_i \in \{1, \dots, K\} \quad (1)$$

where  $K$  is the number of classes including the background. Without much ambiguity, it is convenient to use the same notation  $\bar{y}_i$  for the equivalent *one-hot* distribution

$$\bar{y}_i \equiv (\bar{y}_i^1, \dots, \bar{y}_i^K) \in \Delta_{0,1}^K \quad \text{for} \quad \bar{y}_i^k := [k = \bar{y}_i] \quad (2)$$

where  $[\cdot] \in \{0, 1\}$  is the *True* operator. Set  $\Delta_{0,1}^K$  represents  $K$  possible one-hot distributions, which are vertices of the  $K$ -class *probability simplex*

$$\Delta^K := \{p = (p^1, \dots, p^K) \mid p^k \geq 0, \sum_{k=1}^K p^k = 1\}$$

representing all  $K$ -categorical distributions. The context of each specific expression should make it obvious if  $\bar{y}_i$  is a class index (1) or the corresponding one-hot distribution (2).

Loss functions for scribble-supervised segmentation typically use *negative log-likelihoods* (NLL) over scribbles  $i \in S \subset \Omega$  with ground truth labels  $\bar{y}_i$

$$-\sum_{i \in S} \ln \sigma_i^{\bar{y}_i} \quad (3)$$

where  $\sigma_i = (\sigma_i^1, \dots, \sigma_i^K) \in \Delta^K$  are model predictions at pixels  $i$ . This loss is also standard in full supervision

where  $S = \Omega$ . In this case, no other losses are necessary for training. However, in a weakly supervised setting the majority of pixels are unlabeled, and unsupervised losses are needed for  $i \notin S$ .

The most common unsupervised loss in image segmentation is the Potts model and its relaxations. It is a pairwise loss defined on pairs of *neighboring* pixels  $\{i, j\} \in \mathcal{N}$  for a given neighborhood system  $\mathcal{N} \subset \Omega \times \Omega$ , typically corresponding to the *nearest-neighbor* grid (NN) [7, 19], or other *sparse* (SN) [40] or *dense* neighborhoods (DN) [24]. The original Potts model is defined for discrete segmentation variables, e.g. as in

$$\sum_{\{i,j\} \in \mathcal{N}} P(\sigma_i, \sigma_j) \quad \text{where} \quad P(\sigma_i, \sigma_j) = [\sigma_i \neq \sigma_j]$$

assuming integer-valued one-hot predictions  $\sigma_i \in \Delta_{0,1}^K$ . This *regularization* loss encourages smoothness between the pixels. Its popular *self-supervised* variant is

$$P(\sigma_i, \sigma_j) = w_{i,j} \cdot [\sigma_i \neq \sigma_j]$$

where pairwise affinities  $w_{i,j}$  are based on local intensity edges [7, 19, 24]. Of course, in the context of network training, one should use relaxations of  $P$  applicable to soft predictions  $\sigma_i \in \Delta^K$ . Many forms of such relaxations [35, 45] were studied in segmentation, e.g. *quadratic* [19], *bi-linear* [38], *total variation* [9, 34], and others [15].

Another general unsupervised loss relevant to training segmentation networks is the entropy of predictions, which is also known as *decisiveness* [8, 20]

$$\sum_i H(\sigma_i)$$

where  $H$  is the Shannon’s entropy function. This loss is known to improve generalization and the quality of representation by moving (deep) features away from the decision boundaries [20]. Widely known in the context of unsupervised or semi-supervised classification, this loss also matters in weakly-supervised segmentation where it is used explicitly or implicitly<sup>1</sup>.

Weakly-supervised segmentation methods [10, 22, 33, 41] also use other unsupervised losses (e.g. contrastive), clustering criteria (e.g. K-means), highly-specialized architectures, and ad-hoc training procedures. Our goal is to demonstrate that better results can be easily achieved on standard architectures by combining the standard losses above

$$-\sum_{i \in S} \ln \sigma_i^{\bar{y}_i} + \eta \sum_{i \notin S} H(\sigma_i) + \lambda \sum_{i,j \in \mathcal{N}} P(\sigma_i, \sigma_j). \quad (4)$$

but replacing basic gradient descent optimization [38, 40] by higher-order *self-labeling* techniques [28–30] incorporating optimization of auxiliary *pseudo-labels* as sub-problems.

<sup>1</sup>A unary decisiveness-like term is the difference between quadratic and bi-linear (*tight* but non-convex) relaxations [29, 35] of the Potts model.

## 1.2. Self-labeling and hard pseudo-labels

One motivation for the self-labeling approach to weakly-supervised segmentation comes from well-known limitations of gradient descent for optimizing the Potts relaxations. Even convex relaxations [9, 19, 34] could be challenging in combination with the concave entropy term in (4).

Typical self-labeling methods, including one of the first works on scribble-based semantic segmentation [28], introduce a sub-problem focused on the estimation of *pseudo-labels* for unlabeled points. This subproblem can be formally “derived” from the original network optimization problem or “designed” as a heuristic, see the overview below. We focus on principled auxiliary loss formulations where network parameters and pseudo-labels are jointly optimized in a provably convergent manner. In this case pseudo-labels work as hidden optimization variables simplifying the model estimation, e.g. as in the EM algorithm for GMM.

We denote pseudo-labels  $y_i$  differently from the ground truth labels  $\bar{y}_i$  by omitting the bar. It is important to distinguish them since  $\bar{y}_i$  for  $i \in S$  are given, while  $y_i$  for  $i \in \Omega \setminus S$  are estimated. The majority of existing self-labeling methods [2, 3, 26, 28–30, 42] estimate *hard* pseudo-labels, which could be equivalently represented either by class indices

$$y_i \in \{1, \dots, K\} \quad (5)$$

or by the corresponding one-hot categorical distributions

$$y_i \equiv (y_i^1, \dots, y_i^K) \in \Delta_{0,1}^K \quad \text{for} \quad y_i^k := [k = y_i] \quad (6)$$

analogously with the hard ground truth labels in (1) and (2). In part, hard pseudo-labels are motivated by the network training where the default is NLL loss (3) assuming discrete labels. Besides, powerful discrete solvers for the Potts model are well-known [7, 9, 34]. We discuss the potential advantages of soft pseudo-labels in Section 1.3.

**Overview: joint loss vs “proposal generation”:** Most self-labeling approaches can be divided into two groups. One group designs pseudo-labeling and the network training sub-problems that are not formally related, e.g. [27, 28, 44]. While pseudo-labeling typically depends on the current network predictions and the network fine-tuning uses such pseudo-labels, the lack of a formal relation between these sub-problems implies that iterating such steps does not guarantee any form of convergence. Such methods are often referred to as *proposal generation* heuristics.

Alternatively, the pseudo-labeling sub-problem and the network training sub-problem can be formally derived from a weakly-supervised loss like (4), e.g. by ADM *splitting* [30] or as high-order *trust-region* method [29]. Such methods often formulate a *joint loss* w.r.t. network predictions and pseudo-labels and iteratively decrease the loss. These self-labeling methods are mathematically well-founded, easy to understand and reproduce, and numerically stable due to guaranteed convergence.

### 1.3. Soft pseudo-labels: motivation & contributions

We observe that self-labeling with hard pseudo-labels  $y_i$  is inherently limited as such labels cannot represent the uncertainty of class estimates at unlabeled pixels  $i \in \Omega \setminus S$ . Instead, we focus on *soft* pseudo-labels

$$y_i = (y_i^1, \dots, y_i^K) \in \Delta^K \quad (7)$$

which are general categorical distributions  $p$  over  $K$ -classes. It is possible that the estimated pseudo-label  $y_i$  in (7) could be a one-hot distribution, which is a vertex of  $\Delta^K$ . In this special case,  $y_i$  can be treated as a class index, but we use the general formulation (7) in the main parts of the paper starting Section 2. On the other hand, the ground truth labels  $\bar{y}_i$  are always hard and we use them either as indices (1) or one-hot distributions (2), as convenient.

Soft pseudo-labels can be found in prior work on weakly-supervised segmentation [27, 44] using the “soft proposal generation”. In contrast, we formulate soft self-labeling as a principled optimization methodology where network predictions and soft pseudo-labels are variables in a joint loss, which guarantees convergence of the training procedure. Our pseudo-labels are auxiliary variables for ADM-based [5] splitting of the loss (4) into two simpler optimization sub-problems: one focused on the Potts model over unlabeled pixels, and the other on the network training. While similar to [30], instead of hard, we use soft auxiliary variables for the Potts sub-problem. Our work can be seen as a study of the relaxed Potts sub-problem in the context of weakly-supervised semantic segmentation. The related prior work is focused on discrete solvers fundamentally unable to represent class estimate uncertainty. Our contributions can be summarized as follows:

- convergent *soft self-labeling* framework based on a simple joint self-labeling loss
- systematic evaluation of Potts relaxations and (cross-) entropy terms in our loss
- state-of-the-art in scribble-based semantic segmentation based on standard network architectures (no modifications) and well-founded convergent training procedures that are easy to reproduce and generalize to other problems
- using the same segmentation model, our self-labeling loss with 3% scribbles may outperform standard supervised cross-entropy loss with full ground truth masks.

## 2. Our soft self-labeling approach

First, we apply ADM splitting [5] to weakly supervised loss (4) to formulate our self-labeling loss (8) incorporating additional soft auxiliary variables, i.e. pseudo-labels (7). It is convenient to introduce pseudo-labels  $y_i$  on all pixels in  $\Omega$  even though a subset of pixels (seeds)  $S \subset \Omega$  have ground truth labels  $\bar{y}_i$ . We will simply impose a constraint that pseudo-labels and ground truth labels agree on  $S$ . Thus,

we assume the following set of pseudo-labels

$$Y_\Omega := \{y_i \in \Delta^K \mid i \in \Omega, \text{ s.t. } y_i = \bar{y}_i \text{ for } i \in S\}.$$

We split the terms in (4) into two groups: one includes NLL and entropy  $H$  terms keeping the original prediction variables  $\sigma_i$  and the other includes the Potts relaxation  $P$  replacing  $\sigma_i$  with auxiliary variables  $y_i$ . This transforms loss (4) into expression

$$-\sum_{i \in S} \ln \sigma_i^{\bar{y}_i} + \eta \sum_{i \notin S} H(\sigma_i) + \lambda \sum_{ij \in \mathcal{N}} P(y_i, y_j)$$

equivalent to (4) assuming equality  $\sigma_i = y_i$ . The standard approximation is to incorporate constraint  $\sigma_i \approx y_i$  directly into the loss, e.g. using  $KL$ -divergence. For simplicity, we use weight  $\eta$  for  $KL(\sigma_i, y_i)$  to combine it with  $H(\sigma_i)$  into a single cross-entropy term

$$-\sum_{i \in S} \ln \sigma_i^{\bar{y}_i} + \underbrace{\eta \sum_{i \notin S} H(\sigma_i) + \eta \sum_{i \notin S} KL(\sigma_i, y_i)}_{\eta \sum_{i \notin S} H(\sigma_i, y_i)} + \lambda \sum_{ij \in \mathcal{N}} P(y_i, y_j)$$

defining auxiliary *self-labeling loss* w.r.t. both  $\sigma_i$  and  $y_i$

$$-\sum_{i \in S} \ln \sigma_i^{\bar{y}_i} + \eta \sum_{i \notin S} H(\sigma_i, y_i) + \lambda \sum_{ij \in \mathcal{N}} P(y_i, y_j) \quad (8)$$

approximating the original weakly supervised loss (4).

Iterative minimization of this loss w.r.t. predictions  $\sigma_i$  (model parameters training) and pseudo-labels  $y_i$  effectively breaks the original optimization problem for (4) into two simpler sub-problems, assuming there is a good solver for optimal pseudo-labels. The latter is plausible since the unary term  $H(\sigma_i, y_i)$  is convex for  $y_i$ , and the Potts model (incl. convex and non-convex relaxations) is widely studied.

Section 2.1 discusses standard and new relaxations of the Potts model  $P$ . Section 2.2 discusses several robust variants of the cross-entropy term  $H$  in (8) connecting predictions with uncertain (soft) pseudo-labels  $y_i$  at unlabeled points  $i \in \Omega \setminus S$ . To systematically evaluate these variants of (8) in Section 3, we propose a general efficient GPU-friendly solver for the corresponding pseudo-labeling sub-problem, which is detailed in the Supplementary Material.

### 2.1. Second-order relaxations of the Potts model

We limit our focus to basic second-order relaxations and several motivated extensions. We start from two important standard cases (see Table 1): *quadratic*, the simplest convex relaxation popularized by the *random walker* algorithm [19], and *bi-linear*, which is non-convex but *tight* [35] w.r.t. the original discrete Potts model. The latter implies that optimizing it over relaxed variables should lead to a solution consistent with a discrete Potts solver, e.g. *graph cut* [7] regularizing the geometric boundary of the segments [6]. The quadratic relaxation produces a significantly different soft solution motivated by random walk probabilities [19].

<b>bi-linear</b> $\sim$ "graph cut" $P_{\text{BL}}(p, q) := 1 - p^\top q$	<b>quadratic</b> $\sim$ "random walker" $P_Q(p, q) := \frac{1}{2} \ p - q\ ^2$
<b>normalized quadratic</b> $P_{\text{NQ}}(p, q) := 1 - \frac{p^\top q}{\ p\  \ q\ } \equiv \frac{1}{2} \left\  \frac{p}{\ p\ } - \frac{q}{\ q\ } \right\ ^2$	

Table 1. Second-order Potts relaxations, see Fig.2(a,b,c)

While there are specialized solvers for bi-linear and quadratic relaxations, we are interested in a general efficient pseudo-label solver integrated into the standard GPU-based network optimization framework. This suggests gradient descent as an optimizer for pseudo-labels  $y$  (see Suppl. Mat). Figure 1 shows two representative local minima issues that gradient descent may encounter for (a) the bi-linear and (b) quadratic relaxations of the Potts loss. These examples indicate that gradient descent for these relaxations can distort the properties of the original (discrete) Potts loss.

In (a) two neighboring pixels jointly change the common label from  $y_i = y_j = (1, 0, 0)$  to  $y'_i = y'_j = (0, 1, 0)$ , which corresponds to a "move" where the whole object is reclassified from A to B. This move does not violate the smoothness constraint represented by the original (discrete) Potts model. But, bilinear relaxation prevents move (a) since the intermediate state  $y'_i = y'_j = (\frac{1}{2}, \frac{1}{2}, 0)$  has a higher cost

$$P_{\text{BL}}(y'_i, y'_j) = \frac{1}{2} > 0 = P_{\text{BL}}(y_i, y_j) = P_{\text{BL}}(y''_i, y''_j)$$

while quadratic relaxation assigns constant (zero) loss for all states during this move.

Figure 1(b) shows a move problematic for the quadratic relaxation. Two neighboring pixels on the boundary of objects A and C have labels  $y_i = (1, 0, 0)$  and  $y_j = (0, 0, 1)$ . The second object attempts to change from class label C to B that does not affect the Potts discontinuity penalty between two pixels. But, quadratic relaxation prefers that the second object stays in the intermediate soft state  $y'_j = (0, \frac{1}{2}, \frac{1}{2})$

$$P_Q(y_i, y'_j) = \frac{3}{4} < 1 = P_Q(y_i, y_j) = P_Q(y_i, y''_j)$$

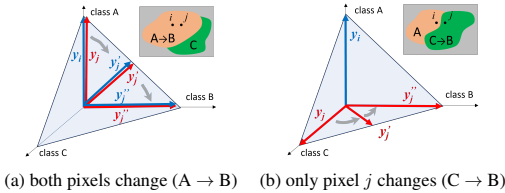


Figure 1. Examples of "moves" for neighboring pixels  $\{i, j\} \in \mathcal{N}$ . Their (soft) pseudo-labels  $y_i$  and  $y_j$  are illustrated on the probability simplex  $\Delta^K$  for  $K = 3$ . In (a) both pixels  $i$  and  $j$  are inside a region/object changing its label from A to B. In (b) pixels  $i$  and  $j$  are on the boundary between two regions/objects; one is fixed to class A and the other changes from class C to B.

<b>collision cross entropy</b> $P_{\text{CC}}(p, q) := -\ln p^\top q$	<b>log-quadratic</b> $P_{\text{LQ}}(p, q) := -\ln \left( 1 - \frac{\ p - q\ ^2}{2} \right)$
<b>collision divergence</b> $P_{\text{CD}}(p, q) := -\ln \frac{p^\top q}{\ p\  \ q\ } \equiv -\ln \left( 1 - \frac{1}{2} \left\  \frac{p}{\ p\ } - \frac{q}{\ q\ } \right\ ^2 \right)$	

Table 2. Log-based Potts relaxations, see Fig.2(d,e,f)

while bi-linear relaxation  $P_{\text{BL}}(y_i, y_j) = 1$  remains constant as  $y_j$  transitions from state C to B.

We propose a new relaxation, *normalized quadratic* in Table 1. Normalization leads to equivalence between quadratic and bi-linear formulations combining their benefits. As easy to check, normalized quadratic relaxation  $P_{\text{NQ}}$  removes the local minima in both examples of Figure 1. Table 2 also proposes "logarithmic" versions of the relaxations in Table 1 composing them with function  $-\ln(1 - x)$ . As illustrated by Figure 2, the logarithmic versions (d-f) address the "vanishing gradients" evident from the flat regions in (a-c).

## 2.2. Cross-entropy and soft pseudo-labels

Shannon's cross-entropy  $H(y, \sigma)$  is the most common loss for training network predictions  $\sigma$  from ground truth labels  $y$  in the context of classification, semantic segmentation, etc. However, this loss may not be ideal for applications where the targets  $y$  are soft categorical distributions representing various forms of class uncertainty. For example, this paper is focused on scribble-based segmentation where the ground truth is not known for most of the pixels, and the network training is done jointly with estimating *pseudo-labels*  $y$  for the unlabeled pixels. In this case, soft labels  $y$  are distributions representing class uncertainty. We observe that if such  $y$  is used as a target in  $H(y, \sigma)$ , the network is trained to reproduce the uncertainty, see Figure 3(a). This motivates the discussion of alternative "cross-entropy" functions where the quotes indicate an informal interpretation of this information-theoretic concept. Intuitively, such functions should encourage decisiveness, as well as proximity between the predictions and pseudo-labels, but avoid mimicking the uncertainty in both directions: from soft pseudo-labels to predictions and vice-versa. We show that the last property can be achieved in a probabilistically principled manner. The following paragraphs discuss three cross-entropy functions  $H$  that we study in the context of our self-labeling loss (8).

**Standard cross-entropy** provides the obvious baseline for evaluating two alternative versions that follow. For completeness, we include its mathematical definition

$$H_{\text{CE}}(y_i, \sigma_i) = H(y_i, \sigma_i) \equiv - \sum_k y_i^k \ln \sigma_i^k \quad (9)$$

and remind the reader that this loss is primarily used with hard or one-hot labels, in which case it is also equivalent to NLL loss  $-\ln \sigma_i^{y_i}$  previously discussed for ground truth labels (3). As mentioned earlier, Figure 3(a) shows that for



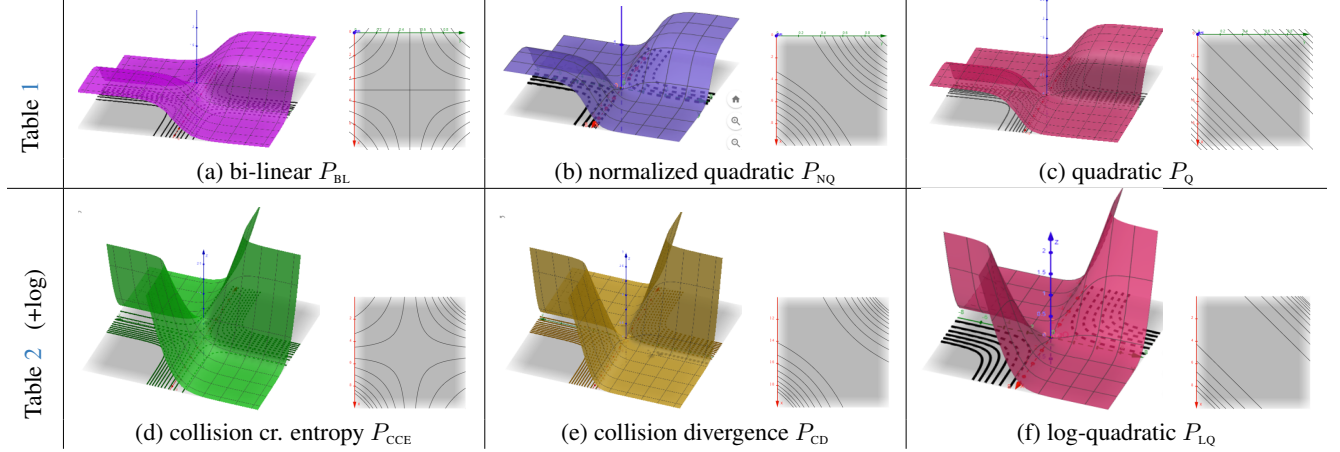


Figure 2. Second-order Potts relaxations in Tables 1 and 2: interaction potentials  $P$  for pairs of predictions  $(\sigma_i, \sigma_j)$  in (4) or pseudo-labels  $(y_i, y_j)$  in (8) are illustrated for  $K = 2$  when each  $\sigma_i$  or  $y_i$  (binary distributions in  $\Delta^2$ ) can be represented by a single scalar as  $(x, 1 - x)$ . The contour maps are iso-levels of  $P((x_i, 1 - x_i), (x_j, 1 - x_j))$  over domain  $(x_i, x_j) \in [0, 1]^2$ . The 3D plots above illustrate the potentials  $P$  as functions over pairs of “logits”  $(l_i, l_j) \in \mathbb{R}^2$  where each scalar  $l_i$  defines binary distribution  $(x_i, 1 - x_i)$  for  $x_i = \frac{1}{1 + e^{-2l_i}} \in [0, 1]$ .

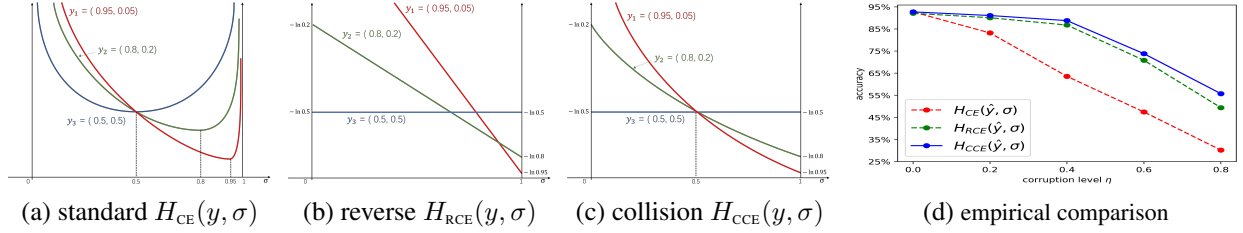


Figure 3. Illustration of cross-entropy functions: (a) standard (9), (b) reverse (10), and (c) collision (11). (d) shows the empirical comparison on the robustness to label uncertainty. The test uses ResNet-18 architecture on fully-supervised *Natural Scene* dataset [32] where we corrupted some labels. The horizontal axis shows the percentage  $\eta$  of training images where the correct ground truth labels were replaced by a random label. All losses trained the model using soft target distributions  $\hat{y} = \eta * u + (1 - \eta) * y$  representing the mixture of one-hot distribution  $y$  for the observed corrupt label and the uniform distribution  $u$ , following [31]. The vertical axis shows the test accuracy. Training with the reverse and collision cross-entropy is robust to much higher levels of label uncertainty.

soft pseudo-labels like  $y = (0.5, 0.5)$ , it forces predictions to mimic or replicate the uncertainty  $\sigma \approx y$ . In fact, label  $y = (0.5, 0.5)$  just tells that the class is unknown and the network should not be supervised by this point. This problem manifests itself in the poor performance of the standard cross-entropy (9) in our experiment discussed in Figure 3 (d) (red).

**Reverse cross-entropy** is defined in this paper as

$$H_{\text{RCE}}(y_i, \sigma_i) = H(\sigma_i, y_i) \equiv - \sum_k \sigma_i^k \ln y_i^k \quad (10)$$

switching the order of labels and predictions in (9), which is not common. Indeed, Shannon’s cross-entropy is not symmetric and the first argument is normally the *target* distribution and the second is the *estimated* distribution. However, in our case, both distributions are estimated and there is no reason not to try the reverse order. It is worth noting that our self-labeling formulation (8) suggests that reverse cross-entropy naturally appears when the ADM approach splits the

decisiveness and fairness into separate sub-problems. Moreover, as Figure 3(b) shows, in this case, the network does not mimic uncertain pseudo-labels, e.g. the gradient of the blue line is zero. The results for the reverse cross-entropy in Figure 3 (d) (green) are significantly better than for the standard (red). Unfortunately, now pseudo-labels  $y$  mimic the uncertainty in predictions  $\sigma$ .

**Collision cross-entropy** defined in this paper as

$$H_{\text{CCE}}(y_i, \sigma_i) \equiv - \ln \sum_k \sigma_i^k y_i^k \equiv - \ln \sigma^\top y \quad (11)$$

resolves the problem in a principled way. It is symmetric w.r.t. pseudo-labels and predictions. The dot product  $\sigma^\top y$  can be seen as a probability of equality of two random variables, the predicted class  $C$  and unknown true class  $T$ , which are represented by the distributions  $\sigma$  and  $y$ . Indeed,

$$\Pr(C = T) = \sum_k \Pr(C = k) \Pr(T = k) = \sigma^\top y.$$

Loss (11) maximizes this “collision” probability instead of enforcing the equality of distributions  $\sigma = y$ . Figure 3(c) shows no mimicking of uncertainty (blue line). Unlike the reverse cross-entropy, this is also valid when  $y$  is estimated from uncertain predictions  $\sigma$  since (11) is symmetric. This leads to the best performance in Figure 3 (d) (blue). Our extensive experiments are conclusive that collision cross-entropy is the best option for  $H$  in self-labeling loss (8).

### 3. Experiments

Our experiments evaluate the components of our loss (8) (cross-entropy, pairwise term, and neighborhood). We compare standard segmentation architectures trained using the “textbook” approach, i.e. loss minimization, to the state-of-the-art methods, which often require network modifications and ad-hoc training procedures. Our quantitative tests in Section 3.1 evaluate different Potts relaxations. Some qualitative examples are presented in Figure 4. Section 3.2 compares three cross-entropy terms. Section 3.3 evaluates our soft self-labeling loss on the nearest-neighbor and dense neighborhood systems. We summarized the results in Section 3.4. Section 3.5 shows that our method achieves the SOTA and, in some cases, may outperform the full supervision.

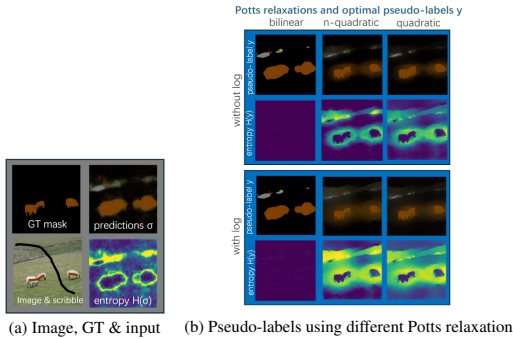


Figure 4. Illustration of the difference among Potts relaxations. The visualization of soft pseudo-labels uses the convex combination of RGB colors for each class weighted by pseudo-label itself.

**Dataset and evaluation** We mainly use the standard PASCAL VOC 2012 dataset [18] and scribble annotations for supervision [28]. The dataset contains 21 classes including background. Following the common practice [11, 37, 38], we use the augmented version with 10,582 training images and 1449 images for validation. Our evaluation metric is the standard mean Intersection-over-Union (mIoU) on the validation set. We also test our method on two additional datasets in Section 3.5. One is Cityscapes [14] which is built for urban scenes and consists of 2975 and 500 fine-labeled images for training and validation. There are 19 out of 30 annotated classes for semantic segmentation. The other one

	scribble length ratio				
	0	0.3	0.5	0.8	1.0
$P_{BL}$	56.42	61.74	63.81	65.73	67.24
$P_{NQ}$	59.01	65.53	67.80	70.63	71.12
$P_Q$	58.92	65.34	67.81	70.43	71.05
$P_{CCE}$	56.40	61.82	63.81	65.81	67.41
$P_{CD}$	59.04	65.52	67.84	70.93	71.22
$P_{LQ}$	59.03	65.44	67.81	70.80	71.21

Table 3. Comparison of Potts relaxations with self-labeling. mIoUs on the validation set are shown here.

is ADE20k [46] which has 150 fine-grained classes. There are 20210 and 2000, images for training and validation. Instead of scribble-based supervision, we followed [27] to use the block-wise annotation as a form of weak supervision.

**Implementation details** We use DeepLabv3+ [13] with two backbones: ResNet101 [21] and MobileNetV2 [36]. We use ResNet101 in Section 3.5, and MobileNetV2 in other sections, for efficiency. We also use Vision Transformer backbone [17], specifically vit-base-patch16-224, and linear decoder in Section 3.5. All backbone networks (ResNet-101 and MobileNetV2, ViT) are pre-trained on Imagenet [16]. Unless stated explicitly, we use batch 12 as the default across all the experiments. To avoid feeding random predictions from the uninitialized classification head into pseudo-labeling sub-problem, we initialize the network using the cross-entropy on scribbles, i.e. the first term in loss (8), similarly to pre-training in [37]. The network parameters are optimized by SGD. The initial learning rate 0.0007 is scheduled by a polynomial decay of power 0.9. All loss variants are optimized for 60 epochs, but all hyperparameters are tuned separately for each variant. For our best result, we use  $\eta = 0.3$ ,  $\lambda = 6$ ,  $H_{CCE}$  and  $P_{CD}$ . The color-bandwidth in the Potts model is set to 9 across all the experiments on Pascal VOC 2012 and 3 for Cityscapes and ADE20k datasets.

#### 3.1. Comparison of Potts relaxations

To compare different Potts relaxations within our self-labeling framework, we select  $H_{CCE}$  as the cross-entropy term in (8), as motivated by the results in Section 3.2. The neighborhood system is the nearest neighbors. The quantitative results are in Table 3. First, one can see that the log-based pairwise terms work consistently better. The likely explanation is that the logarithm addresses the gradient vanishing problem that is obvious in the top row of Figure 2. Moreover, the logarithm encourages smoother transitions across the boundaries (see Figure 4). This may benefit network training when the exact ground truth is unknown. Intuitively, higher uncertainty around object boundaries is natural. Second, the normalized relaxations  $P_{NQ}$  and  $P_{CD}$  work better, confirming the limitations of  $P_{BL}$  and  $P_Q$  discussed in Fig. 1.

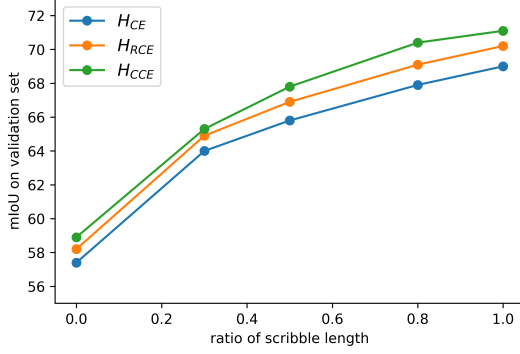


Figure 5. Comparison of cross-entropy terms.

While we focus on a general soft pseudo-label solver (see Suppl.Mat), our results can motivate specialized solvers. For example, quadratic relaxation  $P_Q$  seems attractive as it defines a convex loss (8). If using “quadratic cross-entropy”  $H_Q := \|y - \sigma\|^2$ , then our loss even has a closed-form solution for  $y$  [1, 19]. However, the corresponding pseudo-labels tend to be overly soft and additional *decisiveness* (non-convex entropy) term improves mIoU.

### 3.2. Comparison of cross-entropy terms

We compare different cross-entropy terms while fixing the pairwise term to  $P_Q$  due to its simplicity. We also use the nearest neighbors. The results are in Figure 5. In agreement with Fig.3(d),  $H_{CCE}$  performs consistently better across different supervision levels, i.e. scribble lengths. Both  $H_{CCE}$  and  $H_{RCE}$  have a strong margin over the standard entropy  $H_{CE}$  as network training becomes robust to uncertainty and errors in pseudo labels, see Sec.2.2.

### 3.3. Comparison of neighborhood systems

So far we used the four nearest neighbors (NN) neighborhood for the pairwise Potts term in (8). Here we compare NN with the dense neighborhoods (DN). We use  $H_{CCE}$  as the cross-entropy term. To optimize pseudo-labels over DN, we still use the general gradient descent technique detailed in the Supplementary Material. The gradient computation for DN Potts can employ the efficient *bilateral filtering* [37], but it applies only to (proper) second-order variants, i.e.  $P_{BL}$  and  $P_Q$ . We focus on  $P_Q$  as a preferred option for soft self-labeling. We obtained 71.1% mIoU on nearest neighbors while only getting 67.9% on dense neighborhoods (bandwidth 100). Some qualitative results are shown in Figure 6 indicating that larger neighborhoods induce lower-quality pseudo-labels. A possible explanation is that the Potts model reduces to the cardinality/volume potentials for larger neighborhoods [39]. The nearest neighborhood is better for edge alignment producing better weakly-supervised results.

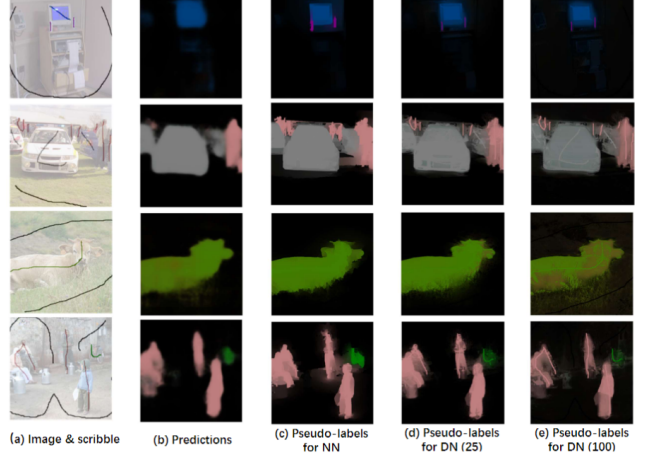


Figure 6. Pseudo-labels generated from given network predictions using different neighborhoods: nearest (NN) and dense (DN).

		$\mathcal{N}$	
		NN	DN
SL	GD	67.0	69.5* [38]
	hard	69.6* [29]	63.1 [28]
	soft	<b>71.1</b>	67.9

Table 4. Summary of Potts-based WSSS (full-scribbles, DeepLab V3+). Reproduced results using public code are marked by \*.

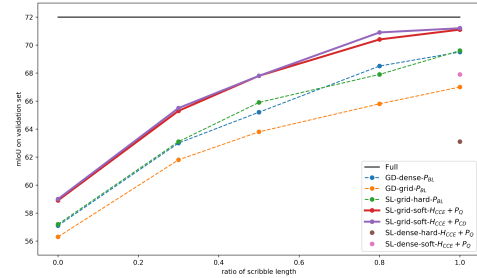


Figure 7. Comparison of different methods using Potts relaxations. The architecture is DeeplabV3+ with the backbone MobileNetV2.

### 3.4. Soft vs. hard self-labeling vs. gradient descent

Here we review our general observations about the Potts-based WSSS using the scribble-based results summarized in Table 4. First, in the simplest approach using direct optimization of the network parameters w.r.t. Potts-regularized losses like (4) and stochastic gradient descent, one benefits from a larger neighborhood size [38]. They use  $P_{BL}$  where DN smoothens the Potts model [30] helping SGD to avoid local minima. Higher-order optimization based on auxiliary self-labeling loss (8) significantly benefits from soft pseudo-labels since they can represent uncertainty. In this case (normalized) quadratic Potts relaxations offer two advantages over the tight bilinear relaxation that leads to hard solutions. On the one hand, they do not suppress label soft-

Method	Architecture	Batchsize	Training Algorithm			$\mathcal{N}$	mIoU
			GD	SL			
				hard	soft		
Full supervision: standard architectures + full masks training (NLL loss)							
Deeplab [12]	V2	12	✓	-	-	-	75.6
Deeplab* [13]	V3+	12	✓	-	-	-	76.6
Deeplab* [13]	V3+	16	✓	-	-	-	78.9
Vision Transformer [17]	ViT-linear	16	✓	-	-	-	81.4
Scribble supervision (full-length scribbles)							
Modified architectures ( $\Delta$ ), and/or ad-hoc self-labeling ( $\circ$ )							
BPG [41]	V2 ( $\Delta$ )	10	✓	-	-	-	73.2
URSS [33]	V2 ( $\Delta$ )	16	✓	-	-	-	74.6
SPML [22]	V2 ( $\Delta$ )	16	✓	-	-	-	74.2
PSI [44]	V3+ ( $\Delta$ )	-	-	-	✓( $\circ$ )	-	74.9
SEMINAR [10]	V3+ ( $\Delta$ )	12	✓	-	-	-	76.2
TEL [27]	V3+	16	-	-	✓( $\circ$ )	-	77.1
AGMM [43]	ViT-linear ( $\Delta$ )	16	-	-	✓( $\circ$ )	-	78.7
Standard architectures + Potts loss optimization (relaxations and/or self-labeling)							
ScribbleSup [28]	V2 (VGG16)	8	-	✓	-	DN	63.1
DenseCRF loss* [38]	V3+	12	✓	-	-	DN	75.8
GridCRF loss* [29]	V3+	12	-	✓	-	NN	75.6
NonlocalCRF loss* [40]	V3+	12	✓	-	-	SN	75.7
$\mathbf{H}_{\text{CCE}} + \mathbf{P}_{\text{Q}}$	V3+	12	-	-	✓	NN	77.5
$\mathbf{H}_{\text{CCE}} + \mathbf{P}_{\text{CD}}$	V3+	12	-	-	✓	NN	77.7
$\mathbf{H}_{\text{CCE}} + \mathbf{P}_{\text{CD}}$ (no pretrain)	V3+	12	-	-	✓	NN	76.7
$\mathbf{H}_{\text{CCE}} + \mathbf{P}_{\text{CD}}$ (no pretrain)	V3+	16	-	-	✓	NN	77.6
$\mathbf{H}_{\text{CCE}} + \mathbf{P}_{\text{CD}}$	V3+	16	-	-	✓	NN	78.1
$\mathbf{H}_{\text{CCE}} + \mathbf{P}_{\text{CD}}$ (no pretrain)	V3+	16	-	-	✓	NN	77.6
$\mathbf{H}_{\text{CCE}} + \mathbf{P}_{\text{CD}}$ (no pretrain)	ViT-linear	12	-	-	✓	NN	80.8
$\mathbf{H}_{\text{CCE}} + \mathbf{P}_{\text{CD}}$ (no pretrain)	ViT-linear	16	-	-	✓	NN	80.94

Table 5. Comparison of scribble-supervised segmentation methods (without CRF postprocessing). We focus on general solutions applicable to any standard architecture based on mathematically well-founded convergent training procedures optimizing a clearly defined loss (the last block). The second block shows specialized solutions based on architectural modifications and/or ad-hoc training procedures that are often non-convergent and hard to reproduce. The numbers are mIoU on the validation dataset of Pascal VOC 2012. The backbone is ResNet101 unless stated otherwise. V2: deeplabV2. V3+: deeplabV3+. ViT-linear: ViT backbone and linear decoder.  $\mathcal{N}$ : neighborhood. “\*”: reproduced results. GD: gradient descent. SL: self-labeling. “no pretrain” means the segmentation network is not pretrained using cross-entropy on scribbles. In some cases (V3+, batch size 12) soft self-labeling outperforms full supervision (see teal color numbers).

ness; this softness is even formally related to classification uncertainty in the random walker method [19]. On the other hand, the convexity of quadratic relaxation does not require DN to simplify loss for gradient descent. Then, it is not surprising that NN works better than DN. The latter makes the Potts model behave as a cardinality potential [39], while in the case of NN the Potts model directly regularized the geometric boundary of objects [6]. Figure 7 also compares these approaches across different scribble lengths.

### 3.5. Comparison to SOTA

This section uses DeepLabV3+ with ResNet101 backbone and ViT-linear transformer to evaluate our self-labeling methodology on these standard architectures and to compare with representative SOTA for scribble-based segmentation. Table 5 presents only the results before any post-processing. Our method may outperform the fully-supervised method (teal color numbers for DeepLabV3+ and batch size 12). Our “text-book” training technique, i.e. minimization of a well-defined loss, applied to standard architectures out-

performs complex WSSS systems requiring architectural modifications and/or ad-hoc multi-stage training procedures.

## 4. Conclusions

This paper proposes a mathematically well-founded self-labeling WSSS framework for standard segmentation networks based on a joint loss (8) w.r.t. network predictions and soft *pseudo-labels*. The latter was motivated as auxiliary variables simplifying optimization of (4). Conceptual properties and systematic evaluation of the terms in our soft self-labeling loss (8) advocate for the *collision cross-entropy* and *collision divergence*. The former replaces the standard cross-entropy  $H$ , and the latter is used as a log of a normalized quadratic relaxation of the Potts model  $P$  over the NN neighborhood. Our general methodology works with any standard architecture and outperforms complex specialized systems based on architectural modifications and/or ad-hoc multi-stage non-convergent training. In contrast, our ideas are easy to understand, reproduce, and extend to other forms of weakly-supervised segmentation (boxes, class tags, etc.).



## References

- [1] Multilabel random walker image segmentation using prior models. In *2005 IEEE computer society conference on computer vision and pattern recognition (CVPR'05)*, pages 763–770. IEEE, 2005. 7, 11
- [2] Jiwoon Ahn and Suha Kwak. Learning pixel-level semantic affinity with image-level supervision for weakly supervised semantic segmentation. In *Proceedings of the IEEE conference on computer vision and pattern recognition*, pages 4981–4990, 2018. 2
- [3] Jiwoon Ahn, Sunghyun Cho, and Suha Kwak. Weakly supervised learning of instance segmentation with inter-pixel relations. In *Proceedings of the IEEE/CVF conference on computer vision and pattern recognition*, pages 2209–2218, 2019. 2
- [4] Nikita Araslanov and Stefan Roth. Single-stage semantic segmentation from image labels. In *Proceedings of the IEEE/CVF Conference on Computer Vision and Pattern Recognition*, pages 4253–4262, 2020. 1
- [5] Stephen Boyd and Lieven Vandenbergh. *Convex optimization*. Cambridge university press, 2004. 3
- [6] Yuri Boykov and Vladimir Kolmogorov. Computing geodesics and minimal surfaces via graph cuts. In *International conference on computer vision (ICCV)*, 2003. 3, 8
- [7] Yuri Y Boykov and M-P Jolly. Interactive graph cuts for optimal boundary & region segmentation of objects in nd images. In *international conference on computer vision (ICCV)*, pages 105–112, 2001. 2, 3
- [8] John Bridle, Anthony Heading, and David MacKay. Unsupervised classifiers, mutual information and phantom targets. *Advances in neural information processing systems*, 4, 1991. 2
- [9] Antonin Chambolle and Thomas Pock. A first-order primal-dual algorithm for convex problems with applications to imaging. *Journal of mathematical imaging and vision*, 40:120–145, 2011. 2
- [10] Hongjun Chen, Jinbao Wang, Hong Cai Chen, Xiantong Zhen, Feng Zheng, Rongrong Ji, and Ling Shao. Seminar learning for click-level weakly supervised semantic segmentation. In *Proceedings of the IEEE/CVF International Conference on Computer Vision*, pages 6920–6929, 2021. 2, 8
- [11] Liang-Chieh Chen, George Papandreou, Iasonas Kokkinos, Kevin Murphy, and Alan L Yuille. Semantic image segmentation with deep convolutional nets and fully connected crfs. *arXiv preprint arXiv:1412.7062*, 2014. 6, 11
- [12] Liang-Chieh Chen, George Papandreou, Iasonas Kokkinos, Kevin Murphy, and Alan L Yuille. Deeplab: Semantic image segmentation with deep convolutional nets, atrous convolution, and fully connected crfs. *IEEE transactions on pattern analysis and machine intelligence*, 40(4):834–848, 2017. 8
- [13] Liang-Chieh Chen, Yukun Zhu, George Papandreou, Florian Schroff, and Hartwig Adam. Encoder-decoder with atrous separable convolution for semantic image segmentation. In *Proceedings of the European conference on computer vision (ECCV)*, pages 801–818, 2018. 6, 8, 11
- [14] Marius Cordts, Mohamed Omran, Sebastian Ramos, Timo Rehfeld, Markus Enzweiler, Rodrigo Benenson, Uwe Franke, Stefan Roth, and Bernt Schiele. The cityscapes dataset for semantic urban scene understanding. In *Proc. of the IEEE Conference on Computer Vision and Pattern Recognition (CVPR)*, 2016. 6, 11
- [15] Camille Couprie, Leo Grady, Laurent Najman, and Hugues Talbot. Power watershed: A unifying graph-based optimization framework. *IEEE transactions on pattern analysis and machine intelligence*, 33(7):1384–1399, 2010. 2
- [16] Jia Deng, Wei Dong, Richard Socher, Li-Jia Li, Kai Li, and Li Fei-Fei. Imagenet: A large-scale hierarchical image database. In *2009 IEEE conference on computer vision and pattern recognition*, pages 248–255. Ieee, 2009. 6
- [17] Alexey Dosovitskiy. An image is worth 16x16 words: Transformers for image recognition at scale. *arXiv preprint arXiv:2010.11929*, 2020. 6, 8
- [18] Mark Everingham, Luc Van Gool, Christopher KI Williams, John Winn, and Andrew Zisserman. The pascal visual object classes (voc) challenge. *International journal of computer vision*, 88:303–308, 2009. 6, 11
- [19] Leo Grady. Random walks for image segmentation. *IEEE transactions on pattern analysis and machine intelligence*, 28(11):1768–1783, 2006. 2, 3, 7, 8, 11
- [20] Yves Grandvalet and Yoshua Bengio. Semi-supervised learning by entropy minimization. *Advances in neural information processing systems*, 17, 2004. 2
- [21] Kaiming He, Xiangyu Zhang, Shaoqing Ren, and Jian Sun. Deep residual learning for image recognition. In *Proceedings of the IEEE conference on computer vision and pattern recognition*, pages 770–778, 2016. 6
- [22] Tsung-Wei Ke, Jyh-Jing Hwang, and Stella X Yu. Universal weakly supervised segmentation by pixel-to-segment contrastive learning. *arXiv preprint arXiv:2105.00957*, 2021. 2, 8
- [23] Alexander Kolesnikov and Christoph H Lampert. Seed, expand and constrain: Three principles for weakly-supervised image segmentation. In *Computer Vision—ECCV 2016: 14th European Conference, Amsterdam, The Netherlands, October 11–14, 2016, Proceedings, Part IV 14*, pages 695–711. Springer, 2016. 1
- [24] Philipp Krähenbühl and Vladlen Koltun. Efficient inference in fully connected CRFs with Gaussian edge potentials. *Advances in neural information processing systems*, 24, 2011. 2
- [25] V. Kulharia, S. Chandra, A. Agrawal, P. Torr, and A. Tyagi. Box2seg: Attention weighted loss and discriminative feature learning for weakly supervised segmentation. In *ECCV'20*. 1
- [26] Jungbeom Lee, Eunji Kim, Sungmin Lee, Jangho Lee, and Sungroh Yoon. Ficklenet: Weakly and semi-supervised semantic image segmentation using stochastic inference. In *Proceedings of the IEEE/CVF Conference on Computer Vision and Pattern Recognition*, pages 5267–5276, 2019. 2
- [27] Zhiyuan Liang, Tiancai Wang, Xiangyu Zhang, Jian Sun, and Jianbing Shen. Tree energy loss: Towards sparsely annotated semantic segmentation. In *Proceedings of the IEEE/CVF Conference on Computer Vision and Pattern Recognition*, pages 16907–16916, 2022. 2, 3, 6, 8, 11

- [28] Di Lin, Jifeng Dai, Jiaya Jia, Kaiming He, and Jian Sun. Scribblesup: Scribble-supervised convolutional networks for semantic segmentation. In *Proceedings of the IEEE conference on computer vision and pattern recognition*, pages 3159–3167, 2016. 1, 2, 6, 7, 8, 11
- [29] Dmitrii Marin and Yuri Boykov. Robust trust region for weakly supervised segmentation. In *Proceedings of the IEEE/CVF International Conference on Computer Vision*, pages 6608–6618, 2021. 2, 7, 8, 11
- [30] Dmitrii Marin, Meng Tang, Ismail Ben Ayed, and Yuri Boykov. Beyond gradient descent for regularized segmentation losses. In *Proceedings of the IEEE/CVF Conference on Computer Vision and Pattern Recognition*, pages 10187–10196, 2019. 2, 3, 7
- [31] Rafael Müller, Simon Kornblith, and Geoffrey E Hinton. When does label smoothing help? *Advances in neural information processing systems*, 32, 2019. 5
- [32] NSD. Natural Scenes Dataset [NSD]. <https://www.kaggle.com/datasets/nitishabharathi/scene-classification>, 2020. 5
- [33] Zhiyi Pan, Peng Jiang, Yunhai Wang, Changhe Tu, and Anthony G Cohn. Scribble-supervised semantic segmentation by uncertainty reduction on neural representation and self-supervision on neural eigenspace. In *Proceedings of the IEEE/CVF International Conference on Computer Vision*, pages 7416–7425, 2021. 2, 8
- [34] Thomas Pock, Antonin Chambolle, Daniel Cremers, and Horst Bischof. A convex relaxation approach for computing minimal partitions. In *IEEE Conference on Computer Vision and Pattern Recognition*, pages 810–817, 2009. 2
- [35] Pradeep Ravikumar and John Lafferty. Quadratic programming relaxations for metric labeling and Markov Random Field MAP estimation. In *The 23rd International Conference on Machine Learning*, page 737–744, 2006. 2, 3
- [36] Mark Sandler, Andrew Howard, Menglong Zhu, Andrey Zhmoginov, and Liang-Chieh Chen. Mobilenetv2: Inverted residuals and linear bottlenecks. In *Proceedings of the IEEE conference on computer vision and pattern recognition*, pages 4510–4520, 2018. 6
- [37] Meng Tang, Abdelaziz Djelouah, Federico Perazzi, Yuri Boykov, and Christopher Schroers. Normalized cut loss for weakly-supervised cnn segmentation. In *Proceedings of the IEEE conference on computer vision and pattern recognition*, pages 1818–1827, 2018. 1, 6, 7, 11
- [38] Meng Tang, Federico Perazzi, Abdelaziz Djelouah, Ismail Ben Ayed, Christopher Schroers, and Yuri Boykov. On regularized losses for weakly-supervised cnn segmentation. In *Proceedings of the European Conference on Computer Vision (ECCV)*, pages 507–522, 2018. 1, 2, 6, 7, 8, 11
- [39] Olga Veksler. Efficient graph cut optimization for full crfs with quantized edges. *IEEE transactions on pattern analysis and machine intelligence*, 42(4):1005–1012, 2019. 7, 8
- [40] Olga Veksler and Yuri Boykov. Sparse non-local crf. In *Proceedings of the IEEE/CVF Conference on Computer Vision and Pattern Recognition*, pages 4493–4503, 2022. 2, 8
- [41] Bin Wang, Guojun Qi, Sheng Tang, Tianzhu Zhang, Yunchao Wei, Linghui Li, and Yongdong Zhang. Boundary perception guidance: A scribble-supervised semantic segmentation approach. In *IJCAI International joint conference on artificial intelligence*, 2019. 2, 8
- [42] Changwei Wang, Rongtao Xu, Shibiao Xu, Weiliang Meng, and Xiaopeng Zhang. Treating pseudo-labels generation as image matting for weakly supervised semantic segmentation. In *Proceedings of the IEEE/CVF International Conference on Computer Vision*, pages 755–765, 2023. 2
- [43] Linshan Wu, Zhun Zhong, Jiayi Ma, Yunchao Wei, Hao Chen, Leyuan Fang, and Shutao Li. Modeling the label distributions for weakly-supervised semantic segmentation. *arXiv preprint arXiv:2403.13225*, 2024. 8
- [44] Jingshan Xu, Chuanwei Zhou, Zhen Cui, Chunyan Xu, Yuge Huang, Pengcheng Shen, Shaoxin Li, and Jian Yang. Scribble-supervised semantic segmentation inference. In *Proceedings of the IEEE/CVF International Conference on Computer Vision*, pages 15354–15363, 2021. 2, 3, 8
- [45] Christopher Zach, Christian Häne, and Marc Pollefeys. What is optimized in tight convex relaxations for multi-label problems? In *IEEE Conference on Computer Vision and Pattern Recognition*, pages 1664–1671, 2012. 2
- [46] Bolei Zhou, Hang Zhao, Xavier Puig, Sanja Fidler, Adela Barriuso, and Antonio Torralba. Scene parsing through ade20k dataset. In *Proceedings of the IEEE conference on computer vision and pattern recognition*, pages 633–641, 2017. 6, 11
- [47] Xiaojin Zhu and Zoubin Ghahramani. Learning from labeled and unlabeled data with label propagation. *ProQuest Number: INFORMATION TO ALL USERS*, 2002. 11

## A. Optimization Algorithm

In this section, we will focus on the optimization of our loss where we iterate the optimization of  $y$  and  $\sigma$ . The network parameters are optimized by standard stochastic gradient descent in all our experiments. Pseudo-labels are also estimated online using a mini-batch. To solve  $y$  at given  $\sigma$ , it is a large-scale constrained convex problem. While there are existing general solvers to find global optima, such as projected gradient descent, it is often too slow for practical usage. Instead, we reformulate our problem to avoid the simplex constraints so that we can use standard gradient descent in PyTorch library accelerated by GPU. Specifically, instead of directly optimizing  $y$ , we optimize a set of new variables  $\{l_i \in \mathbb{R}^K, i \in \Omega\}$  where  $y_i$  is computed by  $\text{softmax}(l_i)$ . Now, the simplex constraint on  $y$  will be automatically satisfied. Note that the hard constraints on scribble regions still need to be considered because the interaction with unlabeled regions through pairwise terms will influence the optimization process. Inspired by [47], we can reset  $\text{softmax}(l_i)$  where  $i \in S$  back to the ground truth at the beginning of each step of the gradient descent.

However, the original convex problem now becomes non-convex due to the Softmax operation. Thus, initialization is important to help find better local minima or even the global optima. Empirically, we observed that the network output logit can be a fairly good initialization. The quantitative comparison uses a special quadratic formulation where closed-form solution and efficient solver [1, 19] exist. We compute the standard soft Jaccard index for the pseudo-labels between the solutions given by our solver and the global optima. The soft Jaccard index is 99.2% on average over 100 images. In all experiments, the number of gradient descent steps for solving  $y$  is 200 and the corresponding learning rate is 0.075. To test the robustness of the number of steps here, we decreased 200 to 100 and the mIoU on the validation set just dropped from 71.05 by 0.72. This indicates that we can significantly accelerate the training without much sacrifice of accuracy. When using 200 steps, the total time for the training will be about 3 times longer than the SGD with dense Potts [38].

## B. Additional Experiments

**Dataset and evaluation** We mainly use the standard PASCAL VOC 2012 dataset [18] and scribble-based annotations for supervision [28]. The dataset contains 21 classes including background. Following the common practice [11, 37, 38], we use the augmented version which has 10,582 training images and 1449 images for validation. We employ the standard mean Intersection-over-Union (mIoU) on validation set as the evaluation metric. We also test our method on two additional datasets. One is Cityscapes [14] which is built for urban scenes and consists of 2975 and 500 fine-labeled

images for training and validation. There are 19 out of 30 annotated classes for semantic segmentation. The other one is ADE20k [46] which has 150 fine-grained classes. There are 20210 and 2000, images for training and validation. Instead of scribble-based supervision, we followed [27] to use the block-wise annotation as a form of weak supervision.

Method	Architecture	Cityscapes	ADE20k
<b>Full supervision</b>			
Deeplab [13]	V3+	80.2	44.6
<b>Block-scribble supervision</b>			
DenseCRF loss [38]	V3+	69.3	37.4
GridCRF loss* [29]	V3+	69.5	37.7
TEL [27]	V3+	71.5	39.2
$\mathbf{H}_{\text{CCE}} + \mathbf{P}_{\text{CD}}$	V3+	72.4	39.7

Table 6. Comparison to SOTA methods (without CRF postprocessing) on segmentation with block-scribble supervision. The numbers are mIoU on the validation dataset of cityscapes [14] and ADE20k [46] and use 50% of full annotations for supervision following [27]. The backbone is ResNet101. “\*”: reproduced results. All methods are trained in a single-stage fashion.